GDCh Research Article Angewandte International Edition Chemie www.angewandte.org

How to cite: Angew. Chem. Int. Ed. 2025, e202423796
doi.org/10.1002/anie.202423796

Battery Cathodes Hot Paper

Tailoring Sodium Carboxymethylcellulose Binders for High-Voltage $LiCoO_2$ via Thermal Pulse Sintering

Shiming Chen[+], Hengyao Zhu[+], Jiangxiao Li, Zu-Wei Yin, Taowen Chen, Xiangming Yao, Wenguang Zhao, Haoyu Xue, Xin Jiang, Yongsheng Li, Hengyu Ren, Jun Chen, Jun-Tao Li, Luyi Yang,* and Feng Pan**

Abstract: Polyvinylidene fluoride (PVDF), as the commercial cathode binder for lithium-ion batteries, presents several practical challenges, including insufficient conductivity, weak adhesion to active materials, and the use of toxic N-methylpyrrolidone for slurry preparation. However, while most water-soluble binders can address the aforementioned issues, they fail to meet the requirements of high-voltage cathodes. In this work, we innovatively employed a thermal pulse sintering strategy to modify carboxymethyl cellulose sodium (CMC), enabling their application in 4.6 V $LiCoO_2$ (93 % capacity retention after 200 cycles). This strategy facilitates the decomposition of electrochemically active carboxyl groups, leading to ring opening reactions that generate numerous ether linkages (-C–O–C-) without introducing undesirable side effects on $LiCoO_2$. The resulting components form additional charge carrier (i.e., Li^+ and e^-) pathways on the cathode surface. Additionally, the heating process also promotes uniform coating of the binder on the surface of $LiCoO_2$, creating a protective layer that inhibits interfacial side reactions. Through proposing a scalable and economic manufacturing technology of multifunctional binder, this work enlightens the avenues for practical high-energy-density batteries.

Introduction

Driven by increasing demands of high-energy-density lithium-ion batteries (LIBs) towards portable electronic devices and electric vehicles, developing the large-capacity cathode with high operating voltage has been greatly paid attention by the academic and industrial circles.[1,2] Layered lithium cobalt oxide ($LiCoO_2$, LCO) as one of the most promising commercial cathode materials in portable devices, exhibits the theoretical capacity up to 274 mAh g^{-1}.[3,4] However, it suffers from serious structural distortion when charged to high voltage (> 4.5 V vs. Li^+/Li), such as reactive oxygen loss, harmful phase transition ($CoO_2 \rightarrow Co_3O_4$) and Co migration.[5–8]

One simple and efficient strategy to improve the cycling stability of high-voltage LCO (HV-LCO) cathode is applied the multifunctional binders which play crucial roles in binding electrode components (i.e., active materials, conductive additives and current collectors).[9] An ideal binder would uniformly cover the surface of LCO particles to form a thin passivation layer, suppressing the decomposition of electrolyte catalyzed by Co active sites.[10] Among commercial binders, polyvinylidene fluoride (PVDF) shows excellent electrochemical stability and has been widely used for high-voltage (HV) cathodes.[11] However, PVDF is relatively costly due to the intrinsic partial fluorination structure (501 \$ kg^{-1}), and requires the use of volatile and toxic N-methyl-2-pyrrolidone (NMP) solvent which results in additional processing costs and is environment-hazardous, hindering its large-scale application.[12] Besides, it has swelled in carbonate-based electrolytes, leading to the worse binding strength with electrode components.[13,14] Hence, it is significant to explore a cost-effective and eco-friendly binder, especially for HV cathode commercial application.[15]

Recently, some designed polymers have been reported as potential binders for HV LCO cathode. For instance, dextran sulfate lithium (DSL) was shown to enhance the stability of Co–O chemical bonds through the sulfate acid groups, suppressing the interfacial side reactions.[10] Alternative organosilicon-type binder enables strong adhesion to LCO surface via hydrogen bonding, and achieves homoge-

[*] S. Chen,[+] H. Zhu,[+] Z.-W. Yin, T. Chen, X. Yao, W. Zhao, H. Xue, X. Jiang, Y. Li, H. Ren, L. Yang, F. Pan
School of Advanced Materials, Peking University Shenzhen Graduate School, Shenzhen 518055, P. R. China
E-mail: yinzuwei@xmu.edu.cn
yangly@pkusz.edu.cn
panfeng@pkusz.edu.cn

H. Zhu[+]
Department of Chemistry, City University of Hong Kong, Kowloon, 999077, Hong Kong

J. Li
National Synchrotron Radiation Laboratory, University of Science and Technology of China, Hefei 230029, P. R. China

Z.-W. Yin, J.-T. Li
College of Energy, Xiamen University, Xiamen, 61005, P. R. China

J. Chen
Institute of Zhejiang, University-Quzhou, Zheda Road 99, Quzhou 324000, P. R. China

[+] These authors contributed equally to this work.

neous coating without self-aggregation during slurry mixing process.[16] However, the above binders face the trouble of a complex synthesis process and are not suitable for large-scale production. In comparison, sodium carboxymethylcellulose (CMC), a water-soluble binder for commercial anodes (i.e., graphite and silicon-based materials),[17–19] exhibits the advantages of safety, environmental friendliness and low price (61 kg^{-1}) vs. PVDF (501 kg^{-1}), which facilitates the large-scale commercialization (Figure S1). Yet, few research has been carried out on the application of CMC binder in HV cathode due to the instability of carboxyl groups (-COOH) under HV condition. Only $LiFePO_4$ cathode (electrochemical testing range: 2.8 V~4.2 V) has been reported with CMC binder, exhibiting satisfactory cycling performance.[20] Hence, the ideal binder for cathodes has been required for low cost, environmental protection, electrochemical inertness and high conductivity.

The thermal pulse sintering (TPS) technique, an extreme non-equilibrium method based on electrical Joule heating, is recognized as a cost-effective and highly efficient strategy for controlling the structure of various functional materials.[21,22] Herein, we employed TPS to remove the electrochemically active functional groups of CMC directly from the LCO electrode for the first time. And the production process is compatible with the existing battery assembly technology, which could facilitate large-scale industrial manufacture and produce a unique micro-nano structure in the cathode (Scheme 1). Abundant -OH and -COOH groups anchor the LCO on the current collector through dehydration reaction during pyrolysis. After controllable TPS process, CMC has been transformed into continuous O-doped carbon networks, enhancing the carrier conductivity (i.e., Li^+ and e^-) and adhesion force with collectors (labeled as CMC-TPS). The obtained cathode with CMC-TPS binder could efficiently protect LCO particles, stabilize the Co–O bond and prevent the Co^{2+} dissolution, improving the structural stability of cathode. This work provides an effective strategy to develop the practical application of HV LCO cathodes.

Results and Discussion

Molecule-Level Electron/Li^+ Network of Modified Binder

To explore the optimal temperature for heat treatment, the thermal decomposition process of pristine CMC was investigated using thermo-gravimetric analysis (TGA) and corresponding differential scanning calorimetry (DSC) under Ar atmosphere (Figure 1a and Figure S2). The main decomposition starts at ~260 °C, which could be attributed to the removal of active functional groups, and slows down after ~500 °C, indicating the carbonization of polymer. Next, a computational quantum chemical approach was used to determine the thermal decomposition path of CMC binder. As an indicator of bond strength, the relaxed force constants R_f (mdyn $Å^{-1}$) of various bonds in CMC monomer were calculated (Figure 1b and Figure S3).[23,24] It is evident that the C–C bonds connecting to the carboxyl and hydroxyl groups on the branch chain have relatively low strength and are more likely to break first during the thermal treatment process. The dynamic bond changes were further confirmed by ab-initio molecular dynamics (AIMD) calculation (Figure 1c and Figure S4). The C–C bond connecting to the carboxyl group breaks preferentially due to the minimum bond energy. Then the bond cleavage of C–C bond (connecting to hydroxyl group on the branch chain) and C–C bond (in six-membered ring) occurs subsequently. To sum up, the ideal thermal decomposition route of CMC could be illustrated (Figure 1d): (1) the ring structure on the

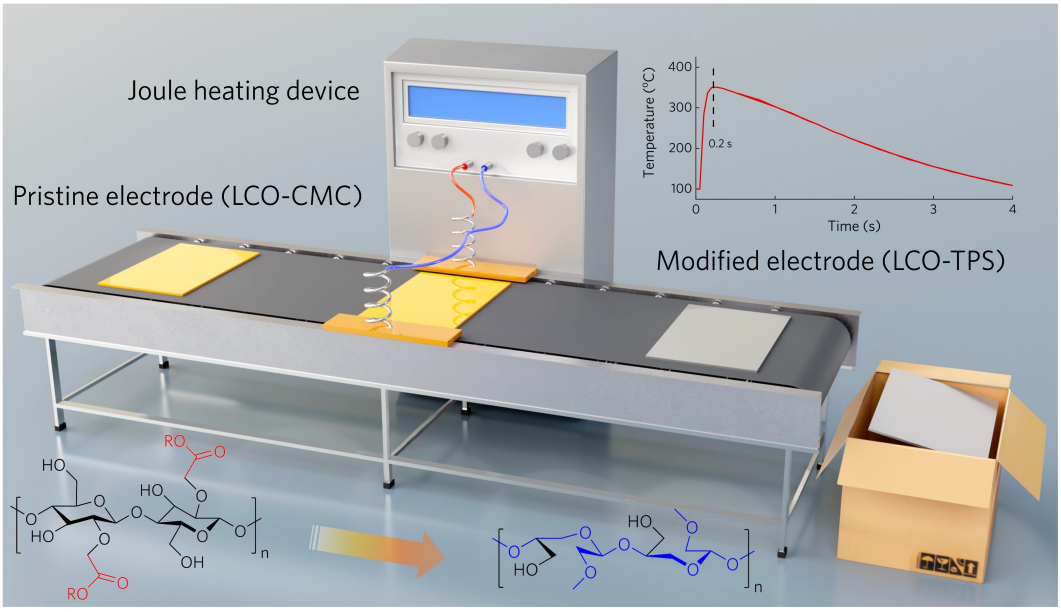

Scheme 1. Schematic illustration of synthesis of LCO-TPS cathode by thermal pulse sintering progress automated continuous production system.

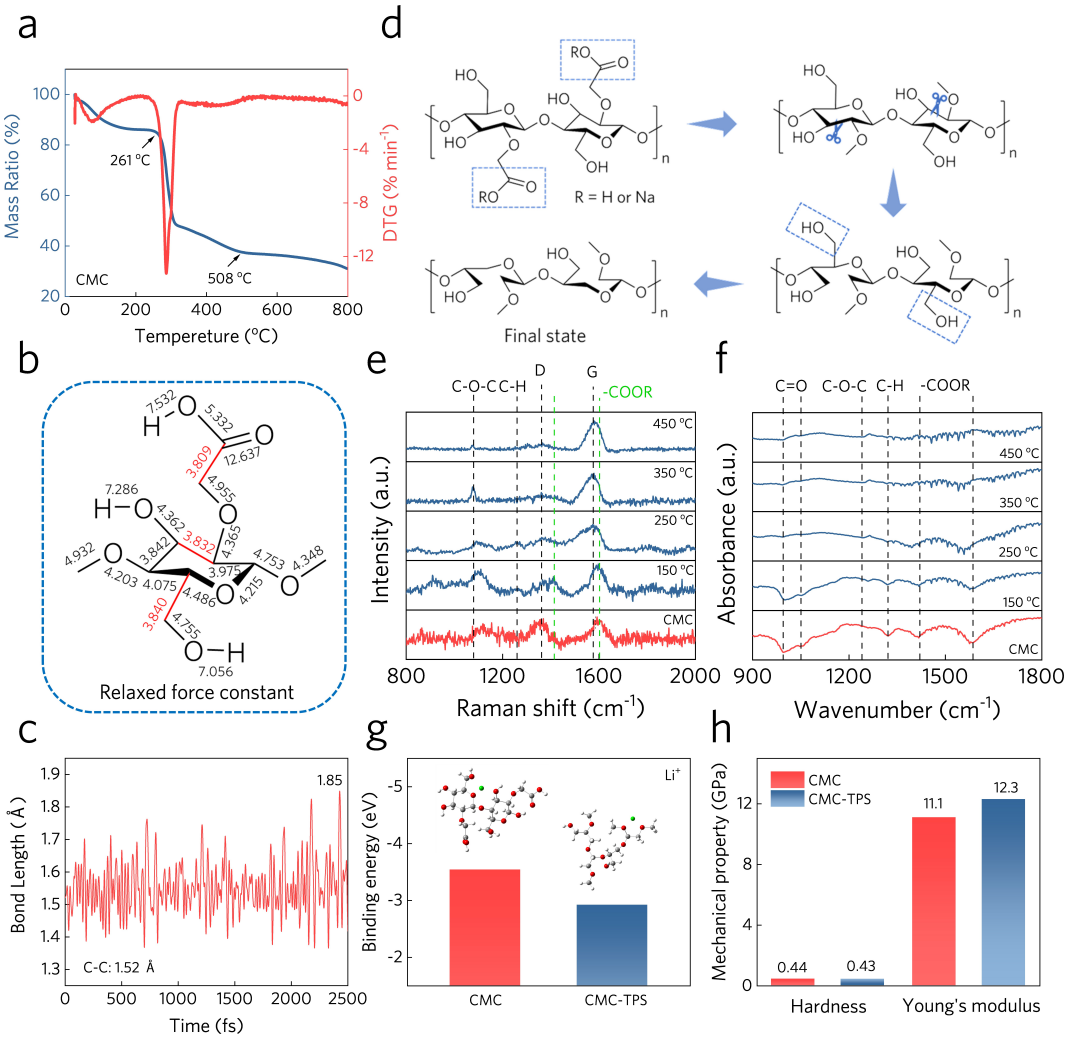

Figure 1. (a) TGA measurement of CMC powder under Ar flow with heating rate of 10 °C min^{-1}; (b) Relaxed force constant of CMC polymer monomer; (c) Bond length of C–C bond connecting to the carboxyl group during the AIMD simulation; (d) Schematic diagram of CMC-TPS polymer formation; (e) Raman spectra and (f) FTIR spectra of CMC binder on Al foil with TPS treatment at various temperature; (g) Binding energy of binders with Li^+; (h) Hardness and Young's modulus of polymer films measured from the nanoindentation test.

main chain undergoes ring-opening and becomes a chain structure rich in ether bonds. (2) the unstable carboxyl groups are clipped and transformed into continuous O-doped carbon networks.

TPS method was applied to modify the molecular structure of CMC binder under various temperatures (Figure S5 and Figure S6). The chemical evolution of CMC during TPS process was examined by Raman (Figure 1e and Figure S7) and Fourier transform infrared (FTIR) spectroscopy (Figure 1f and Figure S8).[25,26] The characteristic Raman peaks at 1415 cm^{-1} and 1610 cm^{-1} that corresponding to the carbonyl stretching vibration of -COOR groups reduced during the TPS process. Furthermore, the D and G bands of carbon emerged at 1350 and 1580 cm^{-1}. Noteworthy, the strong peak at 1075 cm^{-1} corresponded carbohydrate stretches and cyclic respiration (C–O-C) was found at 350 °C cut-off temperature. The FTIR spectra show that the intensity of characteristic peaks at 3286 cm^{-1} (stretch of O–H groups), 1422 cm^{-1}, 1585 cm^{-1} (stretch of COO groups), 1320 cm^{-1} (stretch of C–H groups), 994 cm^{-1} and 1049 cm^{-1} (stretch of C=O groups) gradually weakened and even disappeared with the increasing heating temperature. Combining the results of TGA and spectra, 350 °C was chosen as the appropriate cut-off heating temperature for binder modification. As a result, CMC-TPS binder with rich ether bonds (C–O-C) allows faster Li^+ transport, which is consistent with the results of binding energy with Li^+ (Figure 1g and Figure S9).[27,28] The binding energy between Li^+ and CMC is about −3.45 eV, which is higher than that of CMC-TPS (−2.92 eV). Besides, CMC polymer film with TPS or tube furnace sintering was further compared (Figure S10 and Figure S11). It could be clearly observed that the CMC film sintered by tube furnace has been completely carbonized which is unsuitable for batteries, suggesting the superiority of TPS strategy. The mechanical properties of binders were compared by nanoindentation measurements (Figure 1h and Figure S12). CMC-TPS not only exhibits a higher Young's modulus (12.3 GPa) than that of CMC

(11.1 GPa), but also shows a more uniform hardness distribution.

Physical Characterization of LCO Cathode

High-resolution transmission electron microscopy (HRTEM) was used to visualize the microstructure of different binders on the LCO particles surface (Figure 2a and Figure 2b). The CMC binder displayed a thick, uneven layer with noticeable agglomeration on the LCO cathode (denoted as LCO-CMC). By sharp contrast, a thin layer (~4 nm) is found uniformly covering the LCO surface with the help of TPS process, which is attributed to a higher melt flow index under the large gradient thermal field.[29–31] Besides, the TPS treated LCO electrodes (denoted as LCO-TPS) showed a larger water contact angle (Figure S13), indicating increased hydrophobicity due to the removal of polar groups present in CMC. Consequently, LCO-TPS is expected to absorb less water from the environment, thereby enhancing battery safety and extending cycle life.[32] More importantly, modified CMC binder shows a lower volume resistivity and higher Li^+ conductivity for LCO-TPS electrode than that of LCO-CMC (Figure 2c and Figure S14). According to our previous work,[22] the contact point between the conductive materials will generate more joule heat due to higher resistance, thus forming a local thermal field to accelerate the partial carbonization of binder and finally improving the electronic conductivity of electrodes. The continuous O-doped carbon networks contribute to the transport of carrier.[33,34] Furthermore, the peak intensity ratio of the D (~1350 cm^{-1}) and G (~1590 cm^{-1}) bands ($I_{(D)}/I_{(G)}$) decreased from ~1.15 to ~0.98 in the 2D Raman mapping analysis after the thermal treatment, indicating a higher degree of graphitization and more uniform distribution among the cathode, which is beneficial for the process

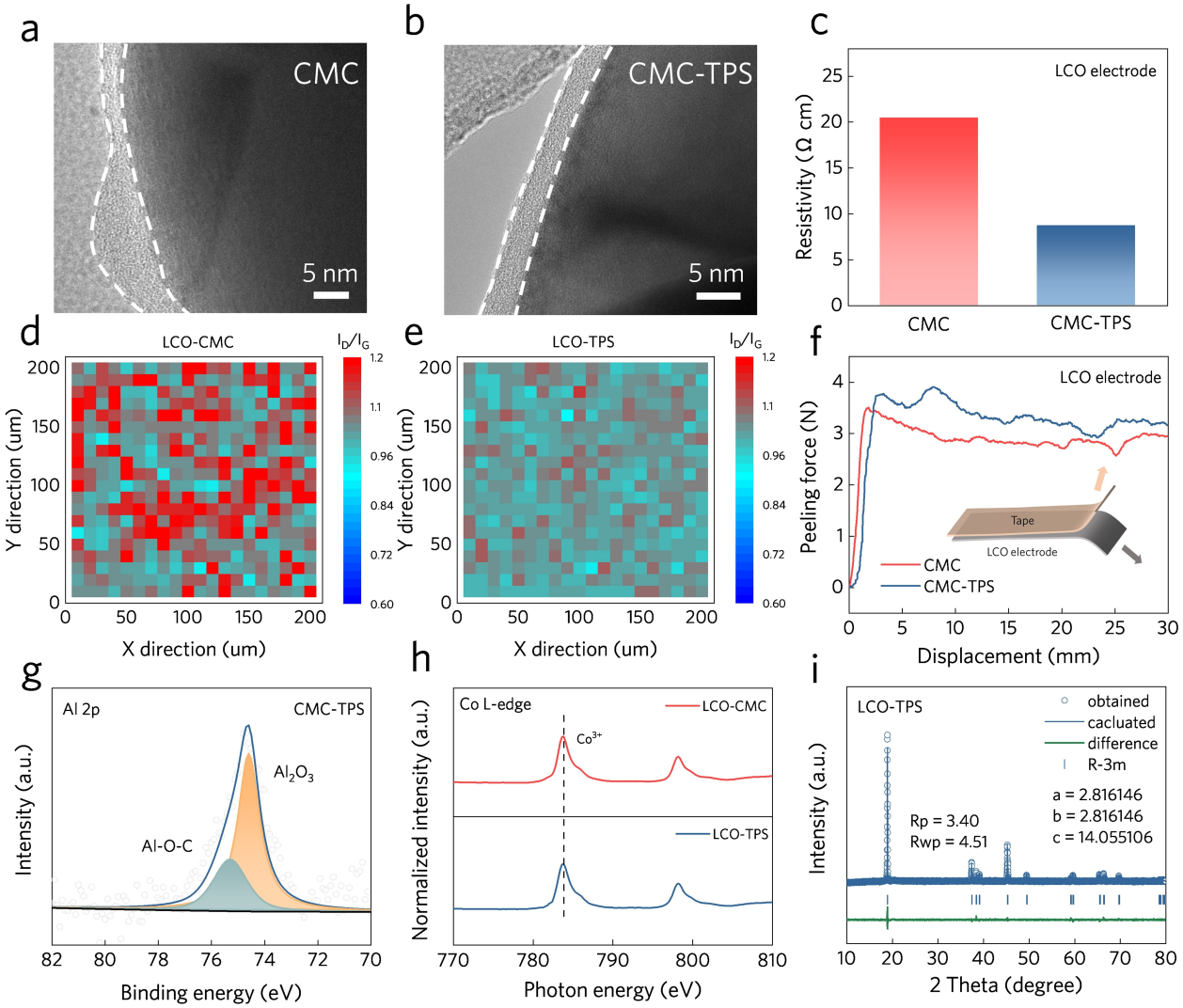

Figure 2. (a) Transmission electron microscopy images of LCO electrodes with CMC (a) and CMC-TPS (b) binder; (c) Resistivity results of LCO-CMC and LCO-TPS cathodes; Mapping of Raman spectra of LCO-CMC (d) and LCO-TPS (e) cathodes; (f) Peeling test results of LCO-CMC and LCO-TPS cathodes; (g) Corresponding Al 2p XPS spectra of LCO-TPS cathode after peeling tests; (h) Co L-edge sXAS results of LCO-CMC and LCO-TPS cathodes; (i) Rietveld refinements of the XRD patterns for LCO-TPS cathodes.

of Li^+ migration (Figure 2d–e and Figure S15). From above, it could be concluded that CMC-TPS binder serves as a robust secondary conductive network within electrodes via molecular-level contact with active material particles.[9]

To evaluate the influence of TPS treatment on the adhesion force for LCO electrodes, peeling tests (180°) were performed (Figure 2f), where LCO-TPS cathode exhibits a detachment force of 3.9 N, higher than that of LCO-CMC (3.4 N). It is revealed that after controllable pyrolysis, abundant -OH and -COOH groups of CMC binder are transformed into continuous O-doped carbon networks between active materials and current collectors, not only constructing the robust conductive network in the electrode but also improving the mechanical adhesive property (Figure 2f).[35] The emerging Al-O–C bonds in Al 2p X-ray photoelectron spectra (XPS, Figure 2g Figure S16 and Figure S17) of LCO-TPS demonstrated that the TPS process helps to form the interfacial chemical bonds with current collector.[36] To verify the universality of CMC-TPS binder for different active materials, the graphite (Gr) anodes loaded on copper (Cu) current collectors were treated by the same strategy. The Cu 2p XPS of electrodes after peeling tests also showed that Cu–O–C bonds were formed between the binder and Cu foil, leading to the superior adhesive property of the Gr-TPS anode (Figure S18 and Figure S19).

Then, the evolution of LCO structure during TPS process was explored, which is vital for practical application. As shown in Figure S20, surface chemical composition and electronic properties of cathodes are explored by XPS. The weaker intensity of C=O peak is found in LCO-TPS cathode due to the decomposition of -COOH groups. In high-resolution Co 2p XPS, two typical peaks at ~780 eV and ~796 eV are ascribed to Co^{3+}, revealing that there is no formation of Co^{2+} after heat treatment (Figure S21). Valence state of Co element was further confirmed by soft X-ray absorption spectroscopy (sXAS) measurement (Figure 2h). In Co L-edge sXAS results, both the spectral shape and energy position of main and shoulder peaks are close for LCO-CMC and LCO-TPS, indicating that Co exists mainly in the form of Co^{3+} ($3d^6$: $t_{2g}^6 e_g^0$).[37,38] To reveal the evolution of surface Co–O bond vibration in LCO cathode, Raman spectra were conducted before and after TPS (Figure S22). The vibration peak at ~490 cm^{-1} corresponds to the O–Co–O bending vibrations (E_g) and the other vibration peak at ~600 cm^{-1} corresponds to the Co–O symmetrical stretching (A_{1g}).[39] It could be found that the peak intensity of E_g and A_{1g} remained similarly during the process, suggesting intact Co–O and O–Co–O bonds on the surface. X-ray diffraction analysis (XRD) refinement could accurately provide the changes of the lattice parameters for LCO cathode. From Figure 2i and Figure S23, the fitted lattice parameters of LCO-CMC and LCO-TPS are nearly the same, indicating the rapid sintering treatment is not able to ruin bulk crystalline structure of LCO, and mainly affects the molecular structure and physical feature of binder. Besides, no cracking was found on the LCO-TPS surface from the scanning electron microscope (SEM) images (Figure S24), showing negligible damage of TPS strategy to LCO cathode.

Enhanced Electrochemical Performance of LCO Cathode

As shown in Figure 3a and Figure 3b, the electrochemical performance of LCO cathodes with CMC binder and CMC-TPS binder (denoted as LCO-TPS) were evaluated by galvanostatic charge–discharge tests in half cells between 3.0 and 4.6 V (*vs* Li/Li^+). LCO-TPS showed a reversible capacity of ~215 mAh g^{-1} at 0.1 C (1 C = 200 mA g^{-1}). By contrast, LCO-CMC not only exhibited a lower capacity (~185 mAh g^{-1}), but also suffered from rapid capacity fading (Figure S25). Both Coulomb efficiency (CE) results and voltage profiles (Figure 3c) showed that pristine CMC binder decomposed seriously under HV operation at 1 C current density. According to the potentiostatic results (Figure S26), the interfacial instability can be attributed to the poor electrochemical stability of -COOH groups in CMC. Besides, replacing -COOH groups with the more stable $-OCH_3$ groups, removing excess -OH groups and extending the terminal groups are able to broaden the electrochemical stability window of binder.[40,41] In the absence of -COOH groups, CMC-TPS enables a higher capacity retention (93 %) after 200 cycles at 1 C, as well as a stabilized CE (Figure 3b). Even with a higher mass loading (~6 mg cm^{-2}), LCO-TPS still showed a reversible capacity of ~210 mAh g^{-1} at 0.2 C with satisfactory cycle stability (Figure S27), indicating the potential of CMC-TPS binder. Next, in situ electrochemical impedance spectroscopy (EIS) of LCO cathodes at the first cycle was carried out to reveal the forming process of cathode electrolyte interphase (CEI) with various binders (Figure 3d and Figure 3e). The CEI impedance (R_{CEI}) and Li^+ transfer resistance (R_{ct}) rapidly increased and during cycling with CMC binder, suggesting the excess interfacial side reactions. On the contrary, the impedance measured in LCO-TPS cathode gradually stabilized and remained stable. Besides, the stabilized interphase for CMC-TPS binder is further confirmed by the EIS results of cycled cells (Figure S28 and Figure S29), where LCO-CMC exhibits a much higher R_{CEI} (15.35 Ω) and R_{ct} (44.56 Ω) than that (8.85 Ω, 17.78 Ω) of LCO-TPS. Moreover, the electrochemical behaviors of graphite (Gr) anodes with different binders were also evaluated in half cells at 0.01–1 V (*vs* Li/Li^+). Gr-TPS anodes exhibited the better cycling stability (corresponding 90 % capacity retention) and rate performance than Gr-CMC anodes (Figure S30 and Figure S31). The EIS plots showed that the Gr-TPS anode exhibited a smaller semicircle and a larger angle from the semicircle to the long-tail profile compared with Gr-CMC anode, suggesting the lower charge-transfer resistance and a faster Li^+ diffusion rate (Figure S32). These results indicate the universality of TPS strategy which transforms CMC into continuous O-doped carbon networks, constructing the robust carrier network of electrode.

Commercially used PVDF was also tested as a benchmark (Figure S33 and Figure S34). The electrochemical results demonstrate that CMC-TPS enhances the cycling

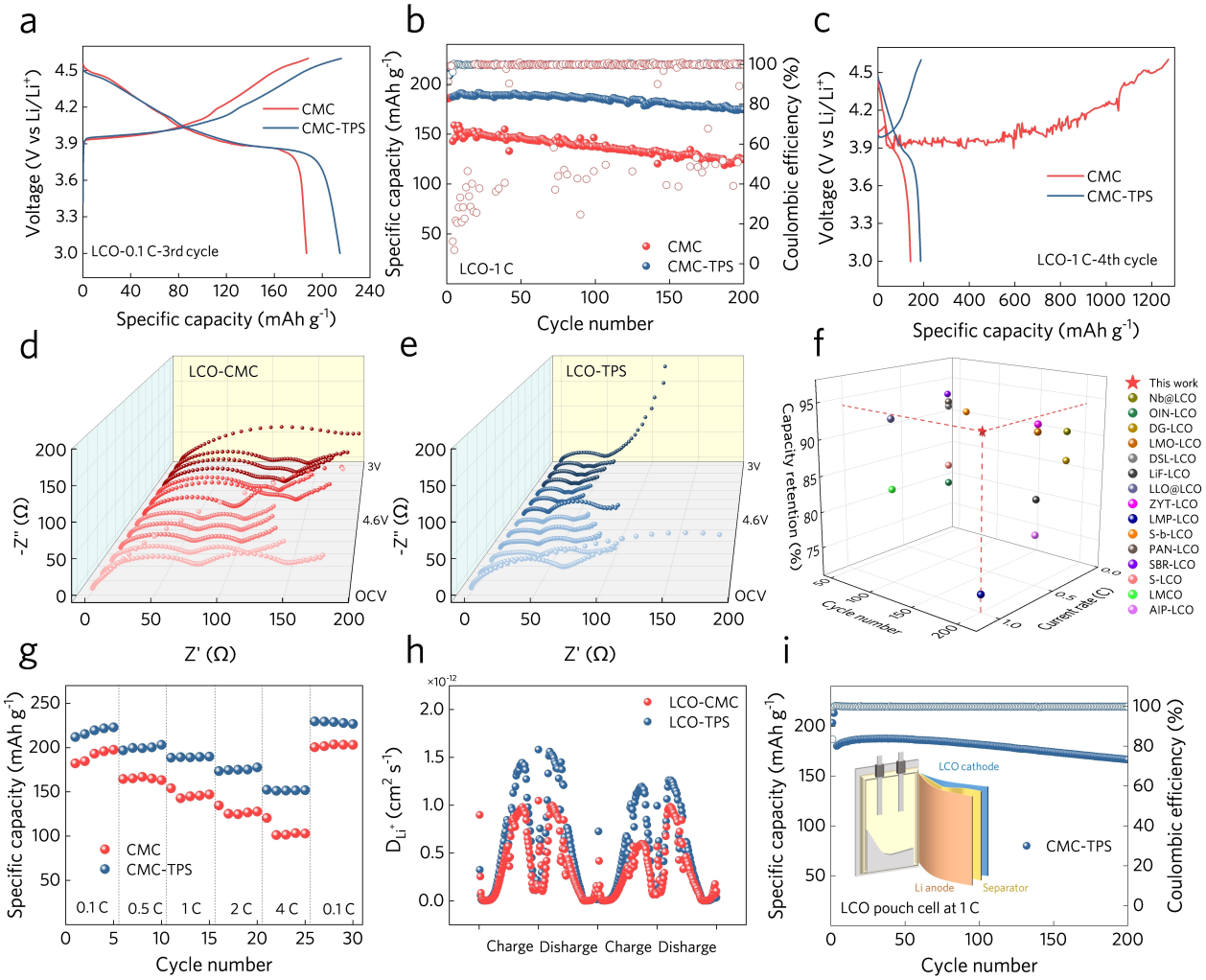

Figure 3. (a) Voltage profiles of LCO||Li cells with various binders for the 3rd cycle; (b) Galvanostatic cycling performance and coulombic efficiency of LCO||Li cells with various binders at a rate of 0.1 C for the first 3 cycles and 1 C for the subsequent cycles; (c) Voltage profiles of LCO||Li cells with various binders for the 4th cycle; In situ EIS of LCO cathodes with CMC (d) and CMC-TPS (e) binders at the first cycle; (f) Electrochemical performance comparison of LCO cathode with various coating layers or binders; (g) Rate performance of LCO||Li cells with various binders; (h) Li^+ diffusion coefficient of LCO cathodes with various binders; (i) Galvanostatic cycling performance and coulombic efficiency of LCO||Li pouch cell at a rate of 1 C with CMC-TPS binder.

stability of LCO comparing with PVDF, highlighting the significant application potential of modified CMC binder. Additionally, in comparison with LCO using other previously reported functional binders (Figure 3f, Figure S35 and Table S1), LCO-TPS exhibited state-of-the-art performance in terms of specific capacity and cycling stability. The rate capability of LCO-CMC and LCO-TPS was also compared (Figure 3g and Figure S36). LCO-CMC exhibited discharge capacities of 185, 167, 145, 125, and 102 mAh g^{-1} at 0.1, 0.5, 1, 2, and 4 C, respectively; while LCO-TPS exhibits superior discharge capacities of 215, 199, 189, 175, and 152 mAh g^{-1}, respectively. The 1st cycle of CV curves at 0.1 mV s^{-1} of various electrodes (Figure S37) showed that the redox peaks of LCO-TPS were sharper than those of LCO-CMC, suggesting a faster Li^+ diffusion kinetics at the surface of LCO-TPS. This speculation is supported by the galvanostatic intermittent titration technique (GITT) results (Figure 3h and Figure S38), where LCO-TPS exhibits higher Li^+ diffusivity. Above results evidently prove the ultrafast Li^+ extraction/insertion kinetics for CMC-TPS system, which could be ascribed to the existence of ether linkages (-C–O–C-) in CMC-TPS binder, since ether linkage was commonly used in the electrolytes to accelerate the ion transport.[27,28] Such results are consistent with the calculations (Figure 1g). As a proof-of-concept demonstration, pouch cell was assembled with LCO-TPS cathode and Li foil anode (~200 μm), and cycled at room temperature in the voltage range of 3.0–4.6 V (*vs* Li/Li^+) at 1 C (Figure 3i). The pouch cell delivered excellent cycling stability (92 %) and maintains a stable voltage plateau during cycling (Figure S39). From above, the LCO-TPS cathode shows the long-term cycling stability and enhanced rate capability at a high cut-off voltage of 4.6 V with the help of a perfect

electron/Li^+ transport network. Besides, the TPS strategy is universal for commercialized graphite anode system.

Stabilized Structure and Interface of LCO Cathode

To reveal the role of CMC-TPS binder in stabilizing HV-LCO, XPS measurements were performed to study the composition of CEI layer. After 200 cycles at 1 C, -CO_3 signal (290.5 eV) is clearly emerged in LCO-CMC cathode compared with the uncycled cathode, suggesting the unrestricted decomposition of carbonate solvents (Figure S20 and Figure S40). Through comparing the F 1s spectra (Figure S41) after cycling, it could be concluded that much larger amounts of LiF was formed in the LCO-TPS cathode derived from the moderate decomposition of $LiPF_6$. By sharp contrast, the interface between the CMC binder and electrolyte experiences the severe and excessive decomposition. The continuous degradation of the interface leads to increasing interfacial resistance (Figure S28) and poor CEI layer.[42,43] Besides, the appearance of Co–O bond (~529 eV) was ascribed to the exposed $LiCoO_2$ particles in CMC system (Figure S42). Time of flight secondary-ion mass spectrometry (TOF-SIMS) was further analyzed the compositional distribution of CEI layer (Figure 4a and Figure S43). For CMC-TPS binder, intense signal of $Li_2F_3^-$ was detected and focused with in a thin layer in the 3D-rendering space, which suggests a dense LiF substance-dominant CEI covered on the LCO cathode derived from the moderate decomposition of $LiPF_6$. Besides, the weaker intensity of C_2HO^- fragments in LCO-TPS demonstrated the suppressed decomposition of carbonate solvents, well agreeing with the XPS results. The minimal presence of CoF_2^- and CoF_3^- fragments in LCO-TPS cathode which are the dissolved products of LCO attacked by electrolyte confirms the controlled side reactions. The microstructure of CEI formed with different binders was further studied by cryo-transmission electron microscopy (cryo-TEM). With the help of CMC-TPS binder, a thin and uniform CEI layer integrally covered the LCO surface, protecting the LCO particles

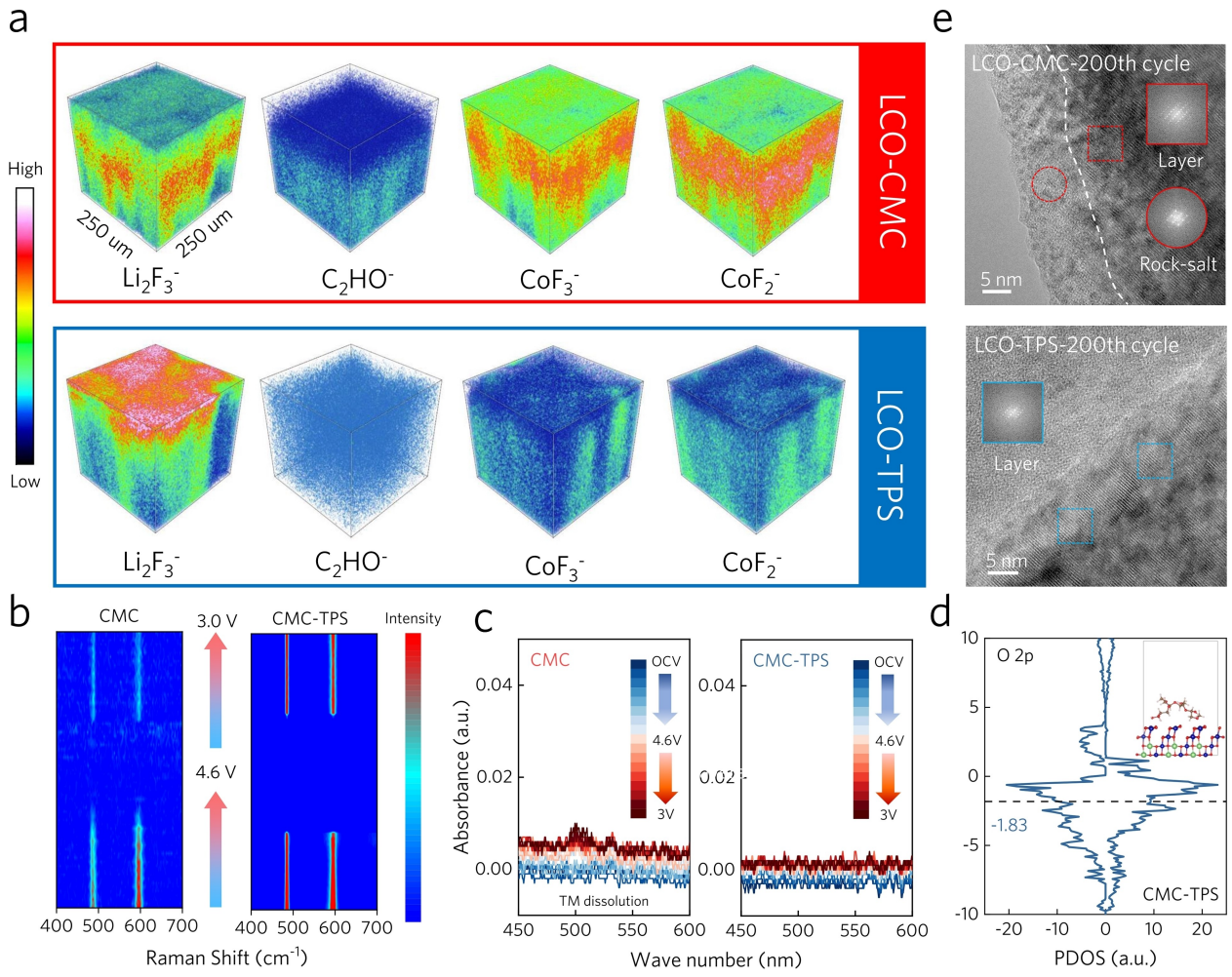

Figure 4. (a) Time of flight secondary-ion mass spectrum (TOF-SIMS) three-dimensional distributions (right) on LCO cathode with various binders after 200 cycles; (b) In situ Raman spectra of LCO||Li cells with various binders in the first cycle; (c) In situ UV/Vis spectra of LCO||Li cells with various binders during cycling; (d) Optimized structure of highly delithiated LCO and corresponding the calculated density of states of O 2p for the outermost single layer of cobalt-oxygen in LCO; (e) HRTEM images of LCO cathodes with various binders after 200 cycles.

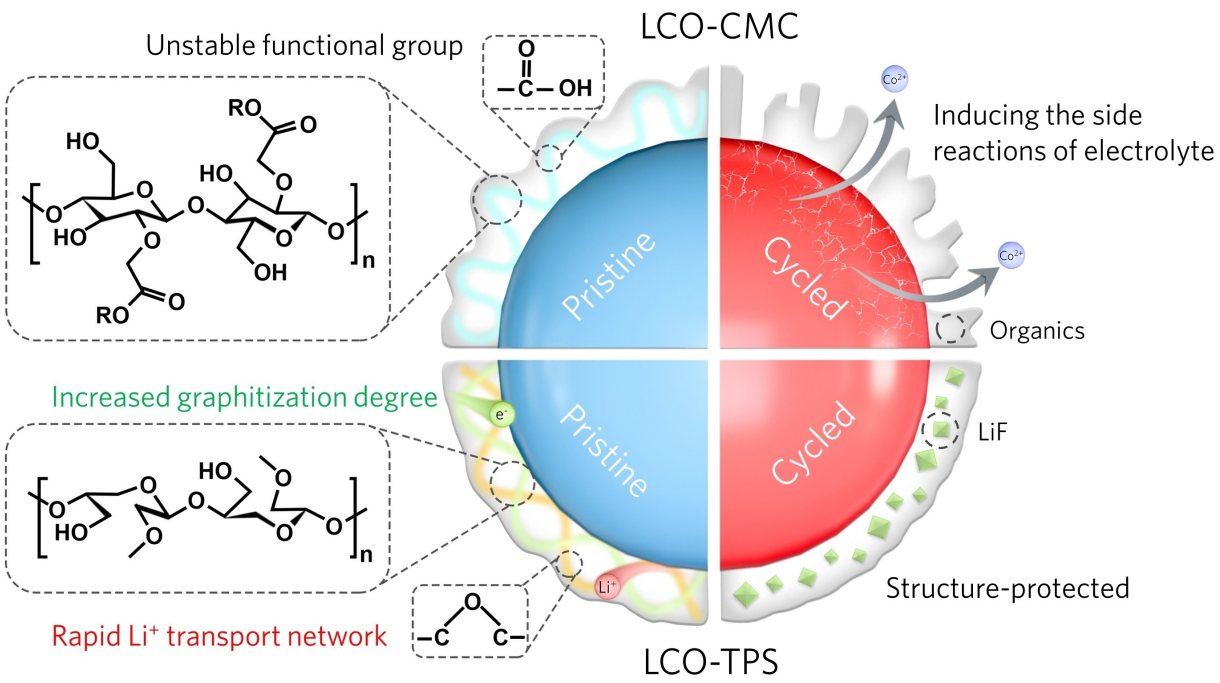

Scheme 2. Schematic illustration of operation mechanism for CMC and CMC-TPS binders.

effectively. By sharp contrast, a broken and thick surface layer was observed in LCO-CMC system (Figure S44).

Next, in situ Raman spectroscopy (Figure 4b) was conducted to analyze the surface bonding of LCO cathode.[44] The strength of Co–O chemical bonds on the LCO surface is closely related to the structural evolution.[10] The intensity of E_g (~485 cm^{-1}) and A_{1g} (~595 cm^{-1}) peaks in the Raman spectra attenuated during the delithiation process, suggesting the weakened Co–O and O–Co–O bonds. Upon re-lithiation, LCO-CMC cathode exhibited dramatic attenuation of E_g and A_{1g} peaks, while LCO-TPS cathode showed superior reversibility of E_g and A_{1g} peaks. Since the fracture of Co–O and O–Co–O bonds in LCO would usually lead to the Co dissolution, in situ ultraviolet-visible (UV/Vis) spectroscopy was employed to measure Co dissolution into the electrolyte (Figure 4c). For LCO-CMC, the absorption peak associated with dissolved Co-ion (~500 nm) emerged and gradually increased in intensity during cycling. By contrast, LCO-TPS shows no apparent absorption peak, demonstrating its capability of suppressing Co dissolution. Furthermore, the Co 2p XPS spectra of cycled Li anodes (Figure S45) also confirmed that Co dissolution from LCO-TPS was greatly constrained. To gain deeper insights of CMC-TPS binder effect at the atomic level, the partial density of states (PDOS) of various delithiated LCO cathodes were compared (Figure 4d and Figure S46). Notably, the O 2p-band center of LCO-TPS shifted to −1.83 eV from −1.69 eV, indicating a significant suppression of redox activity of oxygen anions compared with commercial PVDF binder.[45–47] Additionally, the theoretical adsorption energies of three binders on the LCO surface were compared (Figure S47). CMC-TPS exhibits the higher adsorption energy on LCO (−1.88 eV) than CMC (−1.43 eV) and PVDF (−0.83 eV), indicating superior binding strength with LCO surface.

As shown in Figure 4e, the near-surface structures of LCO cathode were studied by the high-resolution transmission electron microscopy (HRTEM). As expected, the layered structure of LCO particles in LCO-TPS after cycling is well-preserved, in contrast with the serious degradation of surface structure of LCO-CMC cathodes, where a disordered rock-salt phase layer (~10 nm) was formed on the particle surface. Consequently, the crystalline structure of LCO-TPS was better preserved as a relatively lower ratio of H1-3 phase in LCO-TPS (12.5 %) in comparison with LCO-CMC (26.1 %) at 4.6 V (Figure S48). In conclusion, replacing the electrochemically active carboxyl groups (-COOH) with the ether linkages (-C–O-C-) can effectively reduce interfacial side reaction and construct the well-maintained CEI layer with LiF-rich inorganics. In addition, the proposed strategy stabilizes the Co–O bond and crystal structure, and suppresses the Co dissolution of LCO during cycling at high-voltage condition.

Conclusion

In summary, for the first time, based on theoretical calculations, a multifunctional modified CMC binder has been successfully designed and fabricated by a scalable and cost-effective TPS strategy for the high-voltage LCO system. The obtained ether linkage (C–O-C), O-doped carbon network and eliminated carboxyl groups (-COOH) in CMC-TPS not only enables a uniform coating layer on the LCO surface, but also serves as a continuous molecular-level conductive network, improving the carrier (Li^+ and e^-)

conductivity (Scheme 2). Furthermore, such a CMC-TPS binder leads to the formation of stable CEI, stabilization of Co–O bond and crystal structure, alleviation of uncontrolled electrolyte decomposition and Co dissolution, achieving at pouch full-cell level coupled with Li metal anode. This work provides an efficient method of the water-soluble binders for the successful implementation in high-energy-density LIBs. Besides, the commercialization of electrical Joule heating technology could be around the corner under the increasingly attempts being made to improve the experimental apparatus.

Declarations of Competing Interest

The authors declare that they have no known competing financial interests or personal relationships that could have appeared to influence the work reported in this paper.

Acknowledgements

This work was financially supported by the National Key Research and Development Program of China (2022YFB2502103), Shenzhen Science and Technology Research Grant (No. ZDSYS201707281026184), National Natural Science Foundation of China (No. 22309153, No.22288102), Basic public welfare Research Special project of Zhejiang Province (LZY22B040001). The authors thank the support from the XMCD beamline (BL12B) in the National Synchrotron Radiation Laboratory (NSRL) and Shanghai Synchrotron Radiation Facility (SSRF) (beamline 02B02).

Conflict of Interest

The authors declare no conflict of interest.

Data Availability Statement

The data that support the findings of this study are available from the corresponding author upon reasonable request.

Keywords: high-voltage $LiCoO_2$ · CMC binder · thermal pulse sintering · electron and Li^+ transport network

[1] Y. Tian, G. Zeng, A. Rutt, T. Shi, H. Kim, J. Wang, J. Koettgen, Y. Sun, B. Ouyang, T. Chen, Z. Lun, Z. Rong, K. Persson, G. Ceder, *Chem. Rev.* **2021**, *121*, 1623.
[2] J. Xiang, Y. Wei, Y. Zhong, Y. Yang, H. Cheng, L. Yuan, H. Xu, Y. Huang, *Adv. Mater.* **2022**, *34*, 2200912.
[3] Y. Lyu, X. Wu, K. Wang, Z. Feng, T. Cheng, Y. Liu, M. Wang, R. Chen, L. Xu, J. Zhou, Y. Lu, B. Guo, *Adv. Energy Mater.* **2021**, *11*, 1.
[4] J. J. Fang, Y. H. Du, Z. J. Li, W. G. Fan, H. Y. Ren, H. C. Yi, Q. H. Zhao, F. Pan, *J. Electrochem.* **2024**, *30*, 2314005.
[5] L. Wang, B. Chen, J. Ma, G. Cui, L. Chen, *Chem. Soc. Rev.* **2018**, *47*, 6505.
[6] R. Konar, S. Maiti, N. Shpigel, D. Aurbach, *Energy Storage Mater.* **2023**, *63*, 103001.
[7] Z. Zhang, J. Wang, X. Sun, C. Sheng, M. Cheng, H. Liu, Y. Wang, H. Zhou, P. He, *Adv. Funct. Mater.* **2024**, *34*, 2411409.
[8] X. Lin, Y. Sun, Y. Liu, K. Jiang, A. Cao, *Energy Fuels* **2021**, *35*, 7511.
[9] S. Chen, Z. Song, L. Wang, H. Chen, S. Zhang, F. Pan, L. Yang, *Acc. Chem. Res.* **2022**, *55*, 2088.
[10] H. Huang, Z. Li, S. Gu, J. Bian, Y. Li, J. Chen, K. Liao, Q. Gan, Y. Wang, S. Wu, Z. Wang, W. Luo, R. Hao, Z. Wang, G. Wang, Z. Lu, *Adv. Energy Mater.* **2021**, *11*, 2101864.
[11] H. Chen, M. Ling, L. Hencz, H. Y. Ling, G. Li, Z. Lin, G. Liu, S. Zhang, *Chem. Rev.* **2018**, *118*, 8936.
[12] J. Li, R. Klöpsch, S. Nowak, M. Kunze, M. Winter, S. Passerini, *J. Power Sources* **2011**, *196*, 7687.
[13] T. Dong, P. Mu, S. Zhang, H. Zhang, W. Liu, G. Cui, *Electrochem. Energy Rev.* **2021**, *4*, 545.
[14] Y. Zhao, Z. Liang, Y. Kang, Y. Zhou, Y. Li, X. He, L. Wang, W. Mai, X. Wang, G. Zhou, J. Wang, J. Li, N. Tavajohi, B. Li, *Energy Storage Mater.* **2021**, *35*, 353.
[15] J. T. Li, Z. Y. Wu, Y. Q. Lu, Y. Zhou, Q. Sen Huang, L. Huang, S. G. Sun, *Adv. Energy Mater.* **2017**, *7*, 1701185.
[16] J. Ahn, H. Im, Y. Lee, D. Lee, H. Jang, Y. Oh, K. Chung, T. Park, M. Um, J. Woo, J. Kim, D. Jun, J. Yoo, *Energy Storage Mater.* **2022**, *49*, 58.
[17] A. Sano, M. Kurihara, K. Ogawa, T. Iijima, S. Maruyama, *J. Power Sources* **2009**, *192*, 703.
[18] S. Komaba, K. Shimomura, N. Yabuuchi, T. Ozeki, H. Yui, K. Konno, *J. Phys. Chem. C* **2011**, *115*, 13487.
[19] T. W. Kwon, J. W. Choi, A. Coskun, *Chem. Soc. Rev.* **2018**, *47*, 2145.
[20] S. F. Lux, F. Schappacher, A. Balducci, S. Passerini, M. Winter, *J. Electrochem. Soc.* **2010**, *157*, A320.
[21] S. Dou, J. Xu, X. Cui, W. Liu, Z. Zhang, Y. Deng, W. Hu, Y. Chen, *Adv. Energy Mater.* **2020**, *10*, 2001331.
[22] X. Yao, S. Chen, C. Wang, T. Chen, J. Li, S. Xue, Z. Deng, W. Zhao, B. Nan, Y. Zhao, K. Yang, Y. Song, F. Pan, L. Yang, X. Sun, *Adv. Energy Mater.* **2024**, *14*, 2303422.
[23] Y. Tao, W. Zou, S. Nanayakkara, E. Kraka, *J. Chem. Theory Comput.* **2022**, *18*, 1821.
[24] K. Brandhorst, J. Grunenberg, *Chem. Soc. Rev.* **2008**, *37*, 1558.
[25] N. Lv, M. Zhao, L. Hao, X. Zhou, H. Chen, H. Zhou, *Ind. Crops Prod.* **2022**, *190*, 115902.
[26] Y. Cheng, W. Zhu, X. Lu, C. Wang, *Nano Energy* **2022**, *98*, 107229.
[27] M. Zhou, K. Cui, T. S. Wang, Z. Luo, L. Chen, Y. Zheng, B. Li, B. Shi, J. Liu, J. J. Shao, G. Zhou, S. Yang, Y. B. He, *ACS Nano* **2024**.
[28] J. Liu, L. Gao, X. Ruan, W. Zheng, X. Yan, G. He, *Chem. Eng. J.* **2023**, *471*, 144547.
[29] H. Cho, K. Kim, C. M. Park, G. Jeong, *J. Power Sources* **2019**, *410–411*, 25.
[30] J. Kim, S. Lee, S. Jeong, M. Hong, V. C. Ho, Y. D. Park, K. J. Kim, J. Mun, *ChemNanoMat* **2023**, *9*, e202300049.
[31] Y. Jin, H. Yu, X. Liang, *ACS Appl. Mater. Interfaces* **2020**, *12*, 41368.
[32] F. Wang, Y. Wang, Z. Liu, C. Zhang, L. Li, C. Ye, J. Liu, J. Tan, *Adv. Energy Mater.* **2023**, *13*, 2301456.
[33] A. Wang, Y. Tu, S. Wang, H. Zhang, F. Yu, Y. Chen, D. Li, *Polymers (Basel).* **2022**, *14*, 4552.
[34] P. Ding, L. Wu, Z. Lin, C. Lou, M. Tang, X. Guo, H. Guo, Y. Wang, H. Yu, *J. Am. Chem. Soc.* **2023**, *145*, 1548.
[35] N. Yang, J. Sun, R. Shao, Z. Cao, Z. Zhang, M. Dou, J. Niu, F. Wang, *Cell Reports Phys. Sci.* **2022**, *3*, 100862.

[36] F. C. Liu, P. Dong, W. Lu, K. Sun, *Appl. Surf. Sci.* **2019**, *466*, 202.
[37] W. Li, S. Xia, Z. Wang, B. Zhang, B. Li, L. Zhang, K. Qian, J. Ma, X. He, *Appl. Catal. B* **2023**, *325*.
[38] C. Lin, J. Li, Z. W. Yin, W. Huang, Q. Zhao, Q. Weng, Q. Liu, J. Sun, G. Chen, F. Pan, *Adv. Mater.* **2024**, *36*, 2307404.
[39] F. Zhang, N. Qin, Y. Li, H. Guo, Q. Gan, C. Zeng, Z. Li, Z. Wang, R. Wang, G. Liu, S. Gu, H. Huang, Z. Yang, J. Wang, Y. Deng, Z. Lu, *Energy Environ. Sci.* **2023**, *16*, 4345.
[40] X. Yang, M. Jiang, X. Gao, D. Bao, Q. Sun, N. Holmes, H. Duan, S. Mukherjee, K. Adair, C. Zhao, J. Liang, W. Li, J. Li, Y. Liu, H. Huang, L. Zhang, S. Lu, Q. Lu, R. Li, C. V. Singh, X. Sun, *Energy Environ. Sci.* **2020**, *13*, 1318.
[41] Z. Wang, C. Chen, D. Wang, Y. Zhu, B. Zhang, *Angew. Chem. Int. Ed.* **2023**, *62*, e202303950.
[42] X. Shi, T. Zheng, J. Xiong, B. Zhu, Y. J. Cheng, Y. Xia, *ACS Appl. Mater. Interfaces* **2021**, *13*, 57107.
[43] J. Zhang, J. Li, L. Cao, W. Cheng, Z. Guo, X. Zuo, C. Wang, Y. Cheng, Y. Xia, Y. Huang, *Nano Res.* **2024**, *17*, 333.
[44] Chinese Society of Electrochemistry, *J. Electrochem.* **2024**, *30*, 2024121.
[45] Q. Gan, N. Qin, H. Guo, F. Zhang, H. Yuan, W. Luo, Z. Li, Y. Li, L. Lu, Z. Xu, L. Wang, J. Lu, Z. Lu, *ACS Energy Lett.* **2024**, *9*, 1562.
[46] H. Ji, J. Wang, H. Qu, J. Li, W. Ji, X. Qiu, Y. Zhu, H. Ren, R. Shi, G. Ji, W. Zhao, G. Zhou, *Adv. Mater.* **2024**, 2407029.
[47] N. Zhao, Z. Zhang, Z. Wang, Y. Li, Y. Fan, Y. Wang, W. Yan, *Energy Fuels* **2024**, *38*, 16991.

Manuscript received: December 5, 2024
Accepted manuscript online: February 4, 2025
Version of record online: ■■, ■■

Research Article

Battery Cathodes

S. Chen, H. Zhu, J. Li, Z.-W. Yin,* T. Chen, X. Yao, W. Zhao, H. Xue, X. Jiang, Y. Li, H. Ren, J. Chen, J.-T. Li, L. Yang,* F. Pan* _____ **e202423796**

Tailoring Sodium Carboxymethylcellulose Binders for High-Voltage $LiCoO_2$ via Thermal Pulse Sintering

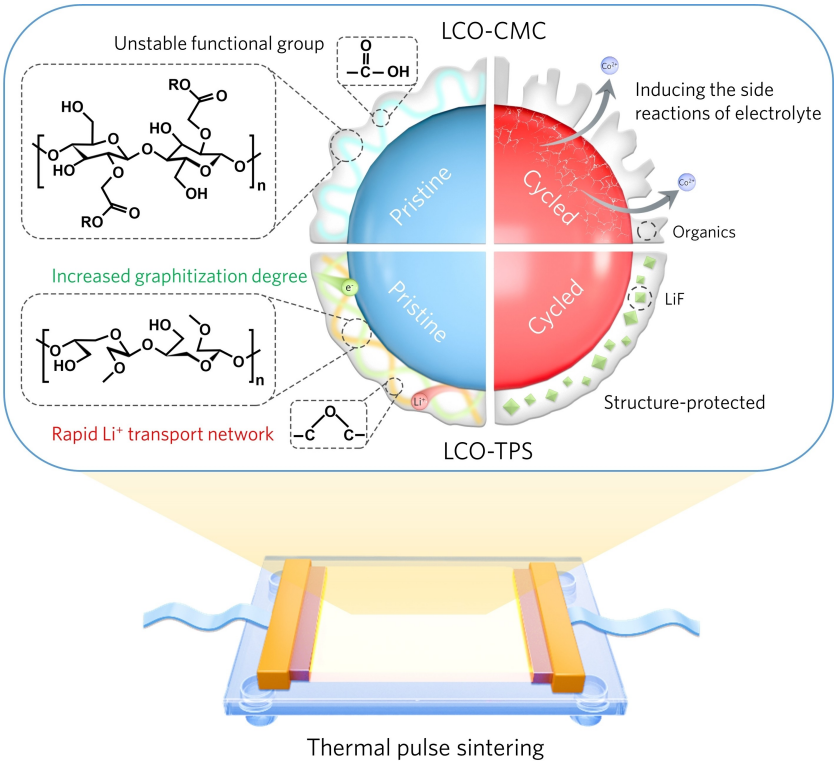

Thermal pulse sintering is proposed to modify carboxymethyl cellulose sodium (CMC) binder by converting carboxyl groups into ether linkages (-C–O–C-). This process produces uniform binder coatings on $LiCoO_2$, forming protective layers and enhancing charge carrier pathways for high-voltage operation, paving the way for scalable and cost-effective multifunctional binder development.